



This is a repository copy of *Mapping and chronology of coversands and dunes from the Aquitaine basin, southwest France*.

White Rose Research Online URL for this paper:
<https://eprints.whiterose.ac.uk/209688/>

Version: Accepted Version

Article:

Bertran, P. orcid.org/0000-0003-3334-9869, Andrieux, E. orcid.org/0000-0003-1688-0543, Bateman, M.D. orcid.org/0000-0003-1756-6046 et al. (3 more authors) (2020) Mapping and chronology of coversands and dunes from the Aquitaine basin, southwest France. *Aeolian Research*, 47. 100628. ISSN 1875-9637

<https://doi.org/10.1016/j.aeolia.2020.100628>

Article available under the terms of the CC-BY-NC-ND licence (<https://creativecommons.org/licenses/by-nc-nd/4.0/>).

Reuse

This article is distributed under the terms of the Creative Commons Attribution-NonCommercial-NoDerivs (CC BY-NC-ND) licence. This licence only allows you to download this work and share it with others as long as you credit the authors, but you can't change the article in any way or use it commercially. More information and the full terms of the licence here: <https://creativecommons.org/licenses/>

Takedown

If you consider content in White Rose Research Online to be in breach of UK law, please notify us by emailing eprints@whiterose.ac.uk including the URL of the record and the reason for the withdrawal request.



eprints@whiterose.ac.uk
<https://eprints.whiterose.ac.uk/>

Mapping and chronology of coversands and dunes from the Aquitaine Basin, southwest France

Pascal Bertran^{1,2*}, Eric Andrieux^{3,4}, Mark D. Bateman⁵, Markus Fuchs⁶, Michael Klinge⁷, Fabrice Marambert¹

*Corresponding author

E-mail address: pascal.bertran@inrap.fr (P. Bertran)

Abstract

New stratigraphic (including GPR profiles) and chronological data provide a detailed understanding of the emplacement of aeolian sands in the Aquitaine basin (SW France). The main phase of coversand deposition ranges from 25 ka to 14 ka. The ages cluster around two periods that match Heinrich events (He-2 and He-1) and reflect increased sedimentation in response to aridification and high mean wind speeds. The age distribution is skewed toward recent phases, which likely results from continuous sand recycling. The dunes currently visible in the landscape were formed during the Younger Dryas/very early Holocene and the historical period. The Younger Dryas dunes are inland low parabolic dunes that have been strongly degraded. Only the last phases of the progression of the coastal dunefield are preserved because of coastal erosion. Two depositional phases have been identified, the Dark Ages Cold Period and the Little Ice Age, which correspond to phases of increased storminess already known from the coastal record in Europe. The Dark Ages Cold Period dunes are high parabolic dunes, whereas the Little Ice Age dunes are predominantly barchanoid. The impact of trampling of the dunes by cattle during the latter period, resulting in reduced vegetation cover, and their artificial stabilization by pine forests seems to be the plausible causes of this morphological difference. Overall, the Aquitaine aeolian system is a good example of a mid-latitude coastal to inland system that was intermittently active during the Quaternary, and where the reconfiguration of the coast following sea level fluctuations played an important role in the chronological distribution of sediments.

Keywords: Pleistocene coversands, Younger Dryas inland dunes, Holocene dunefield, OSL, GPR profiles

1. Introduction

The aeolian system of the Aquitaine Basin (southwest France) is one of the mid-latitude coastal to inland systems that were intermittently active during the Mid and Late Quaternary ([Sun and Muhs, 2013](#)), in a region that is today characterised by temperate (mean annual air temperature of 12.2 to 13°C) and humid (mean annual precipitation of 900 to 1200 mm) climate. The Pleistocene coversands of the Plateau Landais, which is located in the seaward part of the Aquitaine basin, have been the subject of various studies in recent decades with respect to sedimentology, geochemistry and chronology ([Bertran et al., 2011](#), [Sitzia et al., 2015, 2017](#); [Andrieux et al., 2018](#); [Bosq et al., 2019](#)). These studies showed that the coversands form a vast transgressive unit reaching about 13,000 km²,

1 surrounded by a wreath of loess on higher ground (fig. 1). The Plateau Landais is thought to have
2 turned into an aeolian system following the entrenchment during the Quaternary of the surrounding
3 rivers, the Garonne and the Adour, and the subsequent disconnection of the plateau from the
4 hydrographic network. The coversands, which derived from Lower Pleistocene fluvial formations
5 outcropping on the continental shelf exposed during glacial low sea levels, are mainly composed of
6 quartz and other weathering-resistant minerals. They form sheets showing barchanoid and
7 transverse megaripples without avalanche face and with an amplitude of less than one metre. The
8 first chronological data obtained (Bertran et al., 2011, Sitzia et al., 2015) indicate that their
9 accumulation has occurred for at least 400 ka during the Middle and Late Pleistocene glacial periods.
10

11
12 The coversands are overlain by dunes, divided into inland and coastal dunes, the latter forming an
13 approximately continuous dunefield along the Atlantic coast. Some inland dunes have been dated by
14 optical stimulated luminescence (OSL) and yielded either a Younger Dryas (YD) or historical age
15 (Bertran et al., 2011; Sitzia et al., 2015). The coastal dunefield has also been dated by OSL on quartz
16 by Smith et al. (1990) and infrared stimulated luminescence (IRSL) on feldspars by Clarke et al. (1999,
17 2002). The studies have demonstrated the Late Holocene age of the whole dunefield and have
18 highlighted the lack of a clear relationship between age and morphology (parabolic dunes, barchans
19 and barchanoid ridges).
20
21

22
23 Since then, many other ages have been measured in the course of archaeological works at various
24 locations in the coversands and the coastal dunefield, allowing for more detailed understanding of
25 the chronology of aeolian formations. The recent improvement of available digital elevation models
26 (DEMs), in particular the release of the 5 m DEM from the Institut Géographique National (IGN) (RGE
27 ALTI® version 2.0, 5 m resolution) derived from Light Detection And Ranging (LiDAR), has also made a
28 precise determination of dune morphologies possible. At the same time, new stratigraphic data from
29 cross-sections and ground penetrating radar (GPR) profiles were collected. The purpose of this article
30 is to review the recent improvements of the chronostratigraphy of aeolian formations in the
31 Aquitaine Basin, which make it possible to better determine the main depositional phases and their
32 potential controlling factors. To help understand the distribution of the different generations of
33 aeolian accumulations, a map of coversands and dunes was produced using complementary GIS-
34 based approaches.
35
36
37
38
39
40

41 2. Methods

42
43 During archaeological work, trenches were made in the aeolian deposits using an excavator. After
44 manual cleaning of the trenches, the stratigraphy was recorded in detail and samples were taken for
45 dating. In the Castets area, undisturbed profiles of the subsoil structure were also obtained using a
46 GPR (SIR-4000 from Geophysical Survey Systems Inc., GSSI) combined with a 200 MHz antenna
47 (Model 5106) and a survey wheel for distance tracking. Paths were cleaned from wood and ground
48 vegetation between the trees to create an even ground surface ensuring permanent contact
49 between the device and the sediment. The correct transect positions were determined by GPS
50 (Garmin Montana 680T). The data editing and radargram creation was performed using the RADAN 7
51 software from GSSI. The RGE ALTI® 5 m was used to assign elevation data for surface normalization
52 to the radargrams. The recording parameters were: 50 scans per metre, 512 samples per scan,
53 dielectric constant 4.0, maximum depth approx. 16 m.
54
55
56
57
58
59
60
61
62
63
64
65

1 To complete the stratigraphic data obtained from the trenches, logs from boreholes stored in the
2 Banque du Sous-Sol (BSS) of the Bureau des Recherches Géologiques et Minières (BRGM)
3 (<http://infoterre.brgm.fr/>) were consulted. Logs with detailed lithological description were then
4 selected to document the stratigraphy of the Quaternary formations along two representative
5 profiles of the Plateau Landais. All field data were georeferenced and processed in a Geographic
6 Information System (GIS) using the QGIS software (version 3.4).
7

8 For mapping the coversands, we used data from [Bertran et al. \(2016\)](#) with some modifications. The
9 map was created using the soil texture map developed by [Ballabio et al. \(2016\)](#) based on an
10 interpolation of the database from the European project Land Use and Cover Area frame Statistical
11 survey (LUCAS) ([Toth et al., 2013](#)). Pixels (500 m resolution) satisfying the texture range of aeolian
12 sands measured by particle size analysis on a panel of samples were extracted. To remove isolated
13 pixels and generate more continuous surfaces, additional treatment was then applied. The value of
14 each pixel (1: satisfies the aeolian sand texture, 0: does not satisfy the target texture) was
15 recalculated by using the average of the pixel value plus those of the 8 surrounding pixels. Values
16 below the threshold of 0.45 were eliminated. Comparison with the available maps showed that the
17 distribution obtained is in good agreement with that proposed by [Legigan \(1979\)](#) and suggests a
18 greater extension of coversands than that indicated on the BRGM 1:50 000 geological map
19 (<http://infoterre.brgm.fr/>) ([Bertran et al., 2016](#)). The main reason for this extension is the inclusion of
20 areas where the sands are thin (< 2 m) and, therefore, are not recognized in standard geological
21 maps.
22

23 Dune mapping was carried out using the RGE ALTI® 5 m. Extraction of the dune envelope surfaces
24 was carried out according to the following procedure proposed by F. Atilio
25 (<https://www.sigterritoires.fr/index.php/outils-et-methodes/hydrologie/>): (1) construction of a virtual
26 raster with the selected DEM tiles, (2) relief inversion, (3) filling in hollows using the SAGA "fill sinks"
27 tool, (4) relief re-inversion, (5) subtraction of the result from the initial DEM; the reliefs which subsist
28 correspond to terrain higher than the average surface, (6) extraction of the 1 m contours, (7)
29 elimination of contours smaller than a threshold and contours not linked to dunes, (8) assembling the
30 different areas into a single file for the whole area under study, and (9) transforming the contours
31 (1D) into polygons (2D). In areas where the dunes are superimposed on older reliefs, the 2 m or 3 m
32 contours were selected to eliminate parasitic features. The polygons obtained in that way illustrate
33 the distribution of dunes over the whole basin. The maximum and average slopes and the maximum
34 relative elevation were then extracted from the DEM for each polygon. This procedure relying solely
35 on relief had the advantage of simplicity in comparison with more sophisticated tools for automated
36 landform extraction using slope gradient and curvature (e.g. [Drăguț and Blaschke, 2006](#); [Iwahashi
37 and Pike, 2007](#)) and allowed mapping of units of geological interest, i.e. those corresponding to the
38 deposition of substantial sand thicknesses.
39

40 The chronological data for the period 0-100 ka used in this study is a compilation of previously
41 published luminescence ages ([Smith et al., 1990](#); [Bertran et al., 2011](#); [Sitzia et al., 2015](#); [Noppradit et
42 al., 2015](#)) and new luminescence dating from samples collected during recent archaeological
43 excavations. The new samples were prepared and measured in the luminescence laboratories of the
44 University of Sheffield, Royal Holloway (University of London), Durham University and Giessen
45 University, using the methods outlined in Supplementary Information. In order to limit possible
46 biases linked with the heterogeneity of dating methods, the ages from the literature were only
47
48
49
50

considered when obtained using OSL on quartz. Further to this initial filtering, additional efforts were undertaken to re-calculate, when possible, previous luminescence dating using updated parameters and attenuation factors. This reduces the sources of variation between the different datasets and enables comparisons. IRSL ages from feldspars calculated by [Clarke et al. \(1999, 2002\)](#) were used for comparison since they are the only data available for the coastal dunefield, with the exception of the Dune du Pilat ages published by [Smith et al. \(1990\)](#). For older periods (> 100 ka), infrared-radiofluorescence (IR-RF) ages on feldspars and electron spin resonance (ESR) ages on quartz ([Sitzia et al., 2015; Kreutzer et al., 2018; Bosq et al., 2019](#)) were also considered. A total of 98 dates were compiled into the database, out of which 22 were new ([Tables 1, 2](#)).

3. Results

3.1. Mapping and dune morphologies

The map of coversands and dunes is shown in [Figure 1](#). Coversands form a large triangle between the Atlantic Ocean to the west, the Garonne to the north-east and the Adour to the south-east, and cover an area of 11,413 km², which is slightly less than the value proposed by [Bertran et al. \(2011\)](#) probably because of more accurate delineation. The map also shows previously reported sand patches on the plateaus on the right bank of the Garonne north of Bordeaux, which cover approximately 490 km².

Comparison between the dunes identified by the method used in this study and those shown on the BRGM 1:50,000 homogenized geological map shows overall good agreement ([fig. 2A](#)). However, more dunes appear on the new map. The low-relief arms of parabolic dunes, which are clearly visible from the DEM, are poorly captured by the map and sometimes form a series of aligned patches. The dunes are mainly present along the Atlantic coast (coastal dunefield) and south of the parallel 44.7°N passing through the Arcachon lagoon. As previously indicated by [Sitzia et al. \(2017\)](#), inland dunes are concentrated along west-east oriented corridors and on both banks of rivers which are oriented north-south ([fig. 1, 2A-C](#)).

As a general rule, the coastal dunes show strong morphological variations and are structured as follows due to the complex interplay between sand availability, wind strength, vegetation and groundwater table, from the coast to inland ([fig. 3](#)): (1) narrow coastal dune fringe, affected by blowouts from which small parabolic dunes start, (2) isolated to coalescent domed dunes (without avalanche face) and “fat” barchans (see [Parteli et al., 2007](#)) alternating with parabolic dunes, (3) high, often overlapping, barchanoid ridges (which can exceed 30 m in height), (4) isolated barchans, and (5) shallow sand blanket spreading in a zigzag pattern over the Pleistocene surface. Locally, high parabolic dune fields extend ahead of the dunefield ([fig. 2B](#)). These dunes are partially overlapped by the high barchanoid ridges.

Inland dunes are typically elongated, low parabolic dunes (modal height ~4 m), exceptionally exceeding 10 m ([fig. 4](#)), often coalescing. Unlike coastal dunes, the maximum slope is low (mode around 10°) and much lower than the maximum stability slope (32-35°). However, a few dunes are approaching these values. Some of these, close to rivers, are juxtaposed to blowouts that are still clearly visible in topography. This is particularly the case at Rion-des-Landes ([fig. 2D](#)).

3.2. Stratigraphy

Borehole data show that the thickness of the aeolian formations is strongly variable across the basin (fig. 5). In general, the thickness decreases from the shoreline to inland. In the northern part of the basin, which is bounded to the south by the Leyre fault, the thickness occasionally reaches 10 m, except in the coastal dunefield. Trenches excavated at Salaunes showed that the sand thickness can vary rapidly, from less than 0.5 m on the plateau to more than 2 m in filled gullies. At Mios, located close to the fault, the dunes rest directly on Lower Pleistocene fluvial gravel.

To the south, the homogeneous sands found in boreholes, which are ascribed either to the Sable des Landes Formation (aeolian) or to the Castets-Marcheprime Formation in the BSS, can reach up to 30 m in thickness. According to the arguments developed by [Sitzia et al. \(2015\)](#) and [Bosq et al. \(2019\)](#), the Castets-Marcheprime Formation, initially assumed to be fluvial by [Dubreuilh et al \(1995\)](#), does not correspond to a homogeneous chronostratigraphic unit and is of aeolian origin. It is nevertheless possible that the transitional few metres between fluvial gravel at the base of the boreholes (Belin or Onesse-et-Beliet Formations) and purely aeolian sand may correspond to fining-upward fluvial sequences or mixed fluvio-eolian deposits. The lack of accurate description of the sedimentary structures, which would make it possible to determine the depositional environment, does not allow clear conclusions to be drawn.

The schematic stratigraphy of the new sections studied in trenches is shown in [Figure 6](#) and supplements the data provided by [Bertran et al \(2011\)](#) and [Sitzia et al \(2015\)](#). As indicated by these authors, subhorizontally bedded facies predominate in coversands (sandsheet facies) (fig. 7A, B). Units showing crinkly bedding (adhesion ripples) are sometimes interbedded in sands, as well as palaeosols of Histosol, Arenosol and Gleysol type, which are generally cryoturbed. Dune facies include subhorizontal to gently sloping bedded units (aeolian ripple ramps) alternating with steeply sloping cross-bedded units (avalanche faces) (fig. 7C, D).

The GPR profiles carried out at Castets allow determining the structure of the deposits over a thickness of more than 15 m (fig. 8). They show, above a fluvial substrate typified by well-marked reflectors, a unit about 7 m thick with sub-horizontal bedding. According to the borehole BSS002DYHV stored in the BSS, this unit consists of homogeneous sand. It is interpreted as coversands. The coversands are overlain by a parabolic dune up to 8 m high, characterized by predominantly oblique reflectors. The slope of the reflectors locally exceeds 30° and reflects avalanche face stratification. Both profiles show a discontinuity in the stratification, interpreted as a reactivation surface. In the lee side of the dune, the gradient of the strata decreases and becomes progressively sub-parallel to the surface, whose slope does not exceed 15°. The structure thus appears fairly simple and reflects the progression of a single parabolic dune over the Pleistocene coversands, then its degradation.

Because of their height, stratigraphic observations on coastal dunes are more limited. Coastal cliffs are the best available outcrops. The stratigraphy recorded near Soulac (fig. 6) in the northern part of the basin and at the Dune du Pilat ([Froidefont and Legigan, 1985](#); [Bressolier et al., 1990](#)) typically shows (1) at the base, massive, slightly clayey, bioturbed sands of infra-metric thickness sometimes showing preserved horizontal bedding (fig. 7E), resting on Pleistocene coversands or estuarine formations, (2) cross-stratified sands with variable slope, up to 35°. Units with convolute beds, often enriched in organic matter, are also visible (fig. 7F). Lower units are interpreted as shallow sand blanket spreading in front of the dunes, while upper units correspond to the dunes per se. According to the observations of [Bertran et al. \(2011\)](#), convolute bedding resulted from cattle trampling, with

1 footprints sometimes preserved on the bed surface. Successive units are separated by increasingly
 2 poorly developed Histosols/Humic Gleysols and Arenosols towards the top of the sequence.

3.3. Chronology

4
 5 The geographical distribution of dated sites is shown in [Figure 1](#) and the ages are listed in [Table 2](#). A
 6 total of 98 dates were included in our analysis. Among the ages obtained, 45 fall into the Holocene,
 7 39 into the Late Pleistocene-YD and 14 into the Middle Pleistocene. As already noted by [Sitzia et al.](#)
 8 [\(2015\)](#), the distribution is not spatially homogeneous and the northern part of the basin mainly
 9 yielded Middle Pleistocene ages, while the Late Pleistocene and YD ages come from the southern
 10 part ([fig. 9](#)). The new ages support this pattern. According to [Sitzia et al. \(2015\)](#), the main reason is
 11 that the sand sources were mostly coastal during the glacials as they are today, while the
 12 contribution of aeolian sand previously deposited inland was minor owing to armouring by coarse-
 13 grained material, vegetation (although scarce) and/or groundwater table close to the surface.
 14 Widening of the continental shelf to the north and the subsequent remoteness of sand sources
 15 during periods of low sea level from the currently emerged areas best explains why these were not
 16 reached by coversands during the Last Glacial Maximum (LGM).
 17
 18
 19
 20
 21

22 For the period < 100 ka, the chronological distribution of ages was analysed using Kernel Density
 23 Estimation (KDE) and Cumulated Probability Function (CPF) methods ([Vermeesch, 2012](#)). The first
 24 method does not consider the uncertainties associated with the ages but allows a visualisation of
 25 how they cluster. The second method takes into account the distribution of age probability densities
 26 for each age. As a result, CPF tends to disadvantage older ages and those for which uncertainty is
 27 high. Although some pitfalls may affect such a chronological analysis (e.g., [Thomas and Bailey, 2019](#),
 28 and other references herein), we assume here that there is no substantial sampling bias affecting the
 29 age distribution, which thus provides a good approximation of the periods of sand deposition. The
 30 resulting diagram ([fig. 10](#)) highlights the following points:
 31
 32
 33
 34

35 (1) The age distribution is not uniform over time, but phases of high density are distinctly identifiable.
 36 These phases correspond mainly to the Late Pleniglacial and the YD/very early Holocene falling
 37 between ca. 25 ka and 10.5 ka as well as to the Late Holocene. For the older periods, the age density
 38 is low and is probably not representative of the true frequency and timing of aeolian sedimentation.
 39 Three ages around 55 ka come from a single well-dated site (Barp-Pot-aux-Pins, [Sitzia et al., 2015](#)).
 40
 41

42 (2) Peaks in the distribution emerge within these phases. They correspond approximately to cold and
 43 arid periods in western Europe associated with the YD and Heinrich events He-2 and He-1 identified
 44 in marine records ([Bond and Lotti, 1995](#); [Sanchez-Goñi and Harrison, 2010](#)).
 45
 46

47 [Figure 11](#) focuses on the Lateglacial and the Holocene (14-0 ka). This diagram shows the following:
 48
 49

50 (1) Ages between the YD/very early Holocene and the beginning of the historical period are virtually
 51 absent. [Smith et al. \(1990\)](#) obtained an age of 5.4 ka on a shallow unit of bioturbated sands sampled at
 52 the base of the Dune du Pilat. No age earlier than the historical period was provided by cross-
 53 stratified dune sand.
 54
 55

56 (2) Two peaks occur during the historical period using the KDE method for a bandwidth of 0.3 ka, one
 57 at 1.6 ka, the other at 0.4 ka. These peaks correspond to the Little Ice Age (LIA) and the Dark Ages
 58 Cold Period (DACP, [Helama et al., 2017](#), or Early Medieval Dark Ages, EMDA, [Kobashi et al., 2017](#)).
 59 Cumulated age probability densities suggest that the LIA peak could be multi-phased and marked by
 60
 61
 62
 63
 64
 65

at least three distinct sedimentation episodes at 0.82, 0.43 and 0.25 ka respectively. The multi-phased nature of the LIA sedimentation is supported by the presence of weakly developed palaeosols preserved in some dunes (Dune du Pilat: Froidefont and Legigan, 1985; Soulac: Stéphan et al., 2019). Whether these palaeosols developed only locally due to specific conditions or whether they are widespread features remains unknown, however.

(3) The peaks showed by the distribution of IRSL ages obtained by [Clarke et al. \(1999, 2002\)](#) are shifted towards the present with respect to those provided by OSL. Such rejuvenation is probably the result of a methodological issue, caused by differences in the measurement protocol and the lack of correction for fading. Therefore, the peak at 1.12 ka, contemporary to the Medieval Warm Period (MWP), is probably an artifact.

4. Discussion

This study provides new results regarding the mapping and chronology of the sandy aeolian formations of the Plateau Landais. Overall, the coversands are much thinner in the north of the basin than in the south. The Leyre Fault forms approximately the boundary between the two coversand areas. Concomitantly, the coversands 1-2 m depth are Middle Pleistocene in the north and final Late Pleistocene in the south. Plausible explanations for this pattern are:

(1) The southern area was affected by subsidence. According to [Klingebliel and Legigan \(1992\)](#), subsidence is still active with an estimated rate up to 0.5 mm.yr⁻¹ in the Parentis-Biscarosse area. Even though these data should be updated, [Serpelloni et al. \(2013\)](#) suggest significant current downward vertical movements using GPS geodetic measurements. Because of subsidence, the southern area acted as a trap for sand accumulation which through continued to have accommodation space opening up.

(2) As already indicated by [Sitzia et al. \(2015\)](#), lower sea level during the LGM caused the coast to migrate further on the more shallow off-shore platform to the north. Thus aeolian sand would have had to be transported further from sources for it to have been preserved on the presently exposed land-surface. The impacts of sea-level driven coastal reconfiguration on the timing and extent of dune accumulation is well documented from elsewhere, e.g. South Africa ([Bateman et al. 2011](#); [Cawthra et al. 2014](#)). As a result, the sands located at shallow depths under the Holocene soil yield old ages, corresponding to depositional phases associated with a higher sea level than during the LGM. This is in particular obvious for MIS 3 sands, which outcrop to the east of Bordeaux (e.g., Cestas-Pins-de-Jarry, Barp-Pot-aux-Pins). This pattern implies that in the southern part of the basin, Middle Pleistocene sands should be preserved under the younger sediment cover, but have not been observed in outcrops. In agreement with this assumption, a sample taken from the Pontonx quarry yielded an age of 157 ± 16 ka, i.e. Penultimate Glacial, corresponding to a period when sea level drop was close to that of the LGM. The ages obtained by [Andrieux et al. \(2018\)](#) on the aeolian sand fill of ground thermal contraction cracks (sand wedges) at the periphery of coversands indicate, however, that some sand transport was active during the LGM. Sand availability was likely low and did not allow significant accumulation outside of local traps. This pattern was conducive to the formation of ventifact pavements, which have been reported in many locations north of Bordeaux ([Bertran et al., 2011](#)).

The ages obtained on the coversands south of the Leyre fault, from the coast to the eastern limit, show that most of the sediments sampled were deposited between about 25 ka and 14 ka. This

1 phase, corresponding to the maximum coversand extension, overlaps the Greenland stadials GSI-3
 2 and GS-2 (Rasmussen et al., 2014), and matches the main period of aeolian (loess) sedimentation in
 3 other European regions (Antoine et al., 2009; Mezner et al., 2013; Lehmkuhl et al., 2016; Újvári et al.,
 4 2017; Bosq et al., in press). As previously pointed out by Sitzia et al. (2015), coversand emplacement
 5 is older than in the North European Sand Belt, where it did not start until the very end of MIS 2
 6 (Bateman, 1995; Kasse, 1997; Frechen et al., 2001; Kolstrup et al., 2007; Vandenberghe et al., 2013;
 7 Kasse and Aalbersberg, 2019). In these regions, sedimentation was essentially fluvio-eolian before ca.
 8 16 ka (Schokker and Koster, 2004; Zielinski et al., 2015). The main reason suggested was the
 9 existence of permafrost in northern Europe, which limited soil drainage and particle entrainment by
 10 deflation (Schwan, 1987; Kasse, 1997; Sitzia et al., 2015). The release of considerable amounts of
 11 meltwater by the Fennoscandian Ice Sheet during the summers equally played an important role in
 12 the areas close to the ice margin (see Patton et al., 2017, for the reconstruction of glacial drainage).

13
 14 The increased number of available ages in the present study compared to previous ones highlights
 15 well marked peaks in the age distribution. The peaks, which correspond approximately to He-2 and
 16 He-1, indicate that aeolian dynamics was mostly active during the driest and coldest periods of the
 17 Late Pleniglacial because of both vegetation reduction due to aridity and increased wind transport
 18 capacity (Sima et al., 2013; Sitzia et al., 2017; Pinto and Ludwig, 2020).

19
 20 Despite the large uncertainty associated with OSL ages, the hypothesis suggested by Sitzia et al.
 21 (2015) of a continuation of coversand deposition during the early Lateglacial up to the Allerød is not
 22 contradicted by the new age analysis. Samples from two sequences, St-Geours-de-Mareme and
 23 Pindères, show that sandsheet facies yielded Bølling or early Allerød ages, whereas no palaeosol
 24 previously dated by ^{14}C on charcoal provided an age earlier than the second half of the Allerød
 25 (Bertran et al., 2011; Sitzia et al., 2015). As a result, sand stabilisation and colonization by vegetation
 26 was delayed at the beginning of the Lateglacial, probably due to the nutrient deficiency of soils and
 27 the difficulty of plants to resist sand blasting. A similar, albeit shorter delay is also likely at the very
 28 beginning of the Holocene, as indicated by the age obtained at Mios (10.4 ± 0.7 ka) in the
 29 easternmost (downwind) part of the dune.

30
 31 In contrast, the paucity of ages older than 25 ka, especially contemporary to MIS 4 (a period of
 32 considerable dust increase in glacial records, Rasmussen et al., 2014), is puzzling. Several factors, or
 33 more likely a combination of factors, may be involved:

34
 35 (1) Recycling by deflation of previously deposited sands. Some sections (e.g., Pontonx) show that
 36 significant gaps exist in the sediment record. Sand bodies of contrasting ages are separated by flat
 37 erosional surfaces, sometimes lined with small ventifacts, interpreted as deflation surfaces that were
 38 probably controlled by the groundwater table (Fryberger et al., 1988). At Pontonx the sand bodies
 39 above and below the erosional surface were respectively dated to the Late Pleniglacial and the
 40 Penultimate glacial, which implies a gap of over 100 ka. The skewed Late Pleniglacial/Lateglacial age
 41 distribution of the coversands (the older phases are poorly represented in comparison to the
 42 younger) (fig. 10) is assumed to be an effect of recycling. However, although we can envisage that
 43 MIS 4 deposits had been largely recycled during the LGM, it remains difficult to imagine that all these
 44 deposits have been fully eroded where they existed.

45
 46 (2) MIS 4 coversands were of limited extension over the currently emerged continent. The sea level
 47 reached about -90 m at the peak of MIS 4 (Spratt and Lisiecki, 2016) and the coastline underwent
 48 significant reconfiguration. The Middle Pleistocene coversands in the northern part of the basin were
 49
 50
 51
 52
 53
 54
 55
 56
 57
 58
 59
 60
 61
 62
 63
 64
 65

not covered during this period. In contrast, MIS 4 coversands were buried under LGM sediments in the south making them inaccessible by trenching. They are consequently absent from our dataset.

(3) Low aeolian activity occurred during a large part of MIS 4 This would imply that local environmental conditions (soil moisture, vegetation) during MIS 4 were unfavourable to deflation. However, this assumption seems unlikely for the coldest and driest phase of MIS 4, i.e. the GS-19 and GS-18 stadials.

Dating shows that dune formation occurred mainly during a limited number of relatively recent phases, the YD around 12.8 ka for inland dunes and the historical period (1.8-0.2 ka) for coastal and some inland dunes. The YD corresponds to the main phase of inland dune formation in western Europe in areas that were not glaciated ([Bateman and Diez Herrero, 2001](#); [Kasse, 2002](#); [Kasse and Aalbersberg, 2019](#)). The GPR data show that the YD dune of Castets is a simple structure. The avalanche face degraded after the cessation of aeolian dynamics to reach a low value, around 15°, typical of Lateglacial dunes. A discontinuity in the cross stratification suggests that the dune advance could have taken place in two distinct phases. Since no palaeosols were identified in the available sections, these two phases obviously followed one another rapidly.

The transition from the Pleniglacial sandsheet depositional style to the YD low parabolic dunes reflects the role of vegetation, which partially recolonised the landscape during the Allerød. It should be noted that in southern Europe, characterised by a milder climate and a denser LGM shrub vegetation cover ([Strandberg et al., 2011](#)), sandsheet facies are absent and cross-stratified sand units formed during the Last Glacial ([Bosq et al., 2018](#); [Wacha et al., 2019](#)). The conditions specific to the glacial environments of northern Europe, including Aquitaine, i.e. rare vegetation, frozen ground in winter and wet ground during thaw, can, therefore, be identified as the main factor at the origin of the sandsheet facies. Grain-size, mentioned in warm deserts as a decisive factor (sandsheets are usually coarser-grained than dunes, [Kocurek and Nielson, 1986](#)), played no obvious role here since no difference was noted between the grain-size mode of coversands and that of inland dunes ([Sitzia et al., 2017](#)).

The almost complete lack of steeply sloping cross-stratified units within Pleistocene coversands is noteworthy. The only example of a thick (0.9 m) set of oblique beds in between sandsheet facies comes from Fargues-sur-Ourbise in the easternmost part of the coversands ([Sitzia et al., 2015](#)) and has yielded an age of 14.8 ± 0.9 ka, i.e. GI-1e or the very end of GS-2 ([Rasmussen et al., 2014](#)). Whether this dune corresponds to a barchan or a parabolic dune is difficult to determine, however, and its environmental significance remains unknown. This suggests that dunes likely developed repeatedly on the Plateau Landais, but that they have a low preservation potential in the geological record and were mostly destroyed during later glacial phases.

Two main age density peaks emerge during the historical period, one around 1.6 ka, the other around 0.4 ka. These two peaks, which correspond to the DACP and the LIA respectively, have already been well identified in the coastal aeolian record across Europe ([Björck and Clemmensen, 2004](#); [Wilson et al., 2004](#); [Thomas et al, 2008](#); [Costas et al. 2012](#); [Van Vliet-Lanoë et al. 2017](#); [Jackson et al. 2019](#)) and reflect periods of increased storm frequency ([Van Vliet-Lanoë et al. 2014](#); [Auger et al. 2019](#)). The comparison between OSL and IRSL ages suggests that the first IRSL estimates by [Clarke et al. \(2002\)](#) showing a peak around 1.2 ka, i.e. MWP, should not be retained.

Age mapping indicates that the LIA corresponds to high barchanoid dune ridges as well as barchanoid and parabolic dunes located seaward, while the DACP ages come from the high parabolic dune fields located ahead of the former. The distinction between 'primary dunes' and 'modern dunes' locally proposed by different authors (Tastet and Pontee, 1998 and references herein) is thus validated by the new ages and indicates two distinct phases of historical advance of the coastal dunefield. The variability of dune morphologies, only parabolic during the DACP (at least in the area not covered by the LIA dunes) and mostly barchanoid during the LIA, would reflect a less vegetated environment during the second phase. Increased dune vegetation cover is, indeed, the main factor behind their evolution towards a parabolic form (Anthonsen et al., 1996; Hanoch et al., 2018). The factor involved remains difficult to assess, insofar as climatic control can be excluded (the conditions that prevailed during the DACP were not much different from those of the LIA). Section observations indicate that convolute bedding, often showing organic-rich laminae, accounts for a large proportion of dune deposits. This suggests that intensive grazing during the LIA and trampling by cattle may have exerted a major control on vegetation density and aeolian dynamics. Dune trampling is well documented in historical texts (Buffault, 1942, pp. 118-124). Cattle were driven to graze in the interdune areas, locally called "lettes", and were free to wander over the dunes. At that time, the role of grazing as a factor of dune reactivation, which threatened coastal villages, was already strongly debated (Buffault, 1942). An additional factor that may explain the morphological difference between DACP and LIA dunes lies in the much slower stabilization of the former due to natural colonization by vegetation, which promoted a transition from barchanoid to parabolic forms, whereas the latter have been "frozen" with their original shape preserved through artificial stabilization by planting of pine forests during the 19th century (Clarke et al., 2002). Such an evolution has been well documented in the Mu Us dunefield (China) using satellite imagery by Xu et al. (2015). In this dunefield, the growth rate of vegetation, natural or to the contrary controlled by man, had a profound impact on sand transport and was among the main factors of dune evolution.

In many European regions, the ages obtained in coastal dunefields show that other periods were accompanied by the progression of dunes, particularly the late Middle and Late Holocene (see Walker et al., 2019 for the subdivisions of the Holocene Epoch) around 5.5 ka, 4.2 ka and 3.2-2.4 ka (Wilson et al., 2004; Thomas et al., 2008; Costas et al., 2012; Goslin et al., 2019). In Aquitaine, Smith et al. (1990) obtained a single age of 5.4 ka on a thin layer of bioturbated sand at the base of the Dune du Pilat. This sand layer does not correspond to dune deposits per se, but to a sand blanket ahead of a dune according to the pattern currently visible (fig. 3). At Soulac, bioturbated sand with partially preserved horizontal bedding, located underneath cross-stratified dune sand, yielded an age of 1.9 ka. These facies are, therefore, time-transgressive and precede the arrival of dunes in the area under consideration. In the context of considerable retreat of the sandy coast since at least the Late Holocene (Pontee et al., 1998; Stéphane et al., 2019), documented by measurements since the beginning of the 20th century (Buffault, 1942; Aubié et al., 2011), the near absence of ages prior to the historical period must be interpreted as the result of coastal erosion and the subsequent loss of oldest dunes. Only historic dunes currently remain in the landscape.

Some inland dunes have also yielded historical ages (i.e. Rion-des-Landes, Retjons), mostly LIA. These dunes are all located in the immediate vicinity of rivers and to have steep slopes, much steeper than those measured for YD dunes (fig. 12). At Rion-des-Landes, a visual inspection of the DEM also shows that the dunes are connected to blowouts that are still well identifiable (fig. 2D). They reflect the resumption of aeolian activity during the LIA, a feature already identified in other inland sandy areas

elsewhere in Europe (Tolksdorf and Kaiser, 2012; Pierik et al., 2018; de Keyzer and Bateman 2018). As in these areas, it is likely that anthropogenic activity played an important role in dune remobilisation. The blowouts may reflect areas where the protective vegetation cover have been stripped away due to anthropogenic activities. In addition, convolute bedding related to trampling by cattle is abundant at Rion-des-Landes as well as at Retjons (Bertran et al., 2011). Similar facies have also been described in the Netherlands (Koster et al., 1993).

5. Conclusion

The cartographic and chronological study of the aeolian sands of Aquitaine allows us to draw the following conclusions:

(1) Two areas separated by the Leyre Fault and with different depositional histories can be distinguished. The coversands are thin and old (Middle Pleistocene, MIS 3) in the northern area. They were deposited during glacial phases associated with a moderate fall in sea level. Owing to subsidence, the thickness of sand accumulations is greater in the south and the age of subsurface deposits is much younger (Late Pleniglacial, YD). This area is likely to have preserved a detailed record of sedimentation phases during the Middle and Late Pleistocene and should be the focus of future research efforts.

(2) The main phase of coversand emplacement in the south ranges from 25 ka to 14 ka (GS-3 and GS-2). Sedimentation occurred mainly during He-2 and He-1 in response to aridification and high mean wind speeds. The age distribution is skewed toward recent phases because of continuous recycling of the deposits.

(3) The dunes currently visible in the landscape were formed during the YD/very early Holocene (13-10.5 ka) and the historical period. The YD dunes are mainly elongated, low parabolic dunes, which have been strongly degraded.

(4) Only the last phases of progression of the coastal dunefield are preserved because of coastal erosion. Two phases already known elsewhere in Europe have been identified, the DACP and the LIA, which correspond to phases of increased storminess. The MWP phase proposed by Clarke et al (1999, 2002) is probably an artifact due to methodological issues.

(5) The currently exposed DACP dunes are high parabolic dunes, whereas the LIA dunes are predominantly barchanoid. The impact of grazing and trampling of the dunes by cattle during the LIA, resulting in reduced vegetation cover, seems to be a plausible cause of this morphological difference. Artificial stabilization of the LIA dunes by planting of pine forests during the 19th century may also be involved in the preservation of their original barkhanoid shape.

(6) Some inland dunes also developed near rivers during the LIA. They are characterized by steeper slopes and are connected to blowouts still visible in topography.

Section observations allowed the identification of a wide range of palaeosols within the sands. The palaeosols are only preserved locally due to subsequent deflation phases. Therefore, the available data are still too sparse to provide a clear picture of the succession of environments during the Last Glacial. These features merit further investigations.

Shapefiles of the coversand and dune distribution are available on request from the first author (P. Bertran).

Acknowledgements: This study benefited from the financial support of Inrap and the University of Bordeaux. We would like to thank the archaeologists who provided access to the sites, notably L. Bourguignon, J.F. Chopin, B. Ducournau, V. Elisagoyen, P. Fouéré and A. Pons-Méthois, as well as the assistant scientific and technical director L. Detrain. D. Sauer is also acknowledged for help in the field. The OSL dating work in this study was undertaken in different laboratories as outlined in the SI. We thank the institutions (University of Sheffield, Durham University and Royal Holloway, University of London, Justus-Liebig University of Giessen) and in particular S. Armitage for providing us access to the Luminescence equipment. S. Armitage also participated to the improvement of the text. The two anonymous reviewers are also greatly acknowledged for their constructive remarks on the manuscript.

References

- Aubié, S., Mallet, C., Favennec, J., Hoareau, A., 2011. Caractérisation de l'aléa érosion (2020-2040) de la côte aquitaine dans le cadre de l'étude stratégique de gestion du trait de côte. Observatoire de la côte Aquitaine, rapport final. Unpublished report, Bureau de Recherches Géologiques et Minières, Orléans, BRGM/RP-59095-FR.
- Andrieux, E., Bateman, M., Bertran, P., 2018. The chronology of Late Pleistocene thermal contraction cracking derived from sand wedge dating in central and southern France. *Global and Planetary Change* 162, 84-100.
- Anthonsen, K.L., Clemmensen, L.B., Jensen, J.H., 1996. Evolution of a dune from crescentic to parabolic form in response to short-term climatic changes: Rabjerg Mile, Skagen Odde, Denmark. *Geomorphology* 17, 63-77.
- Antoine, P., Rousseau, D.-D., Moine, O., Kunesch, S., Hatté, C., Lang, A., Tissoux, H., Zöller, L., 2009. Rapid and cyclic aeolian deposition during the Last Glacial in European loess: a high-resolution record from Nussloch, Germany. *Quaternary Science Reviews* 28, 2955–2973.
- Auger, J.D., Mayewski, P.A., Maasch, K.A., Schuenemann, K.C., Carleton, A.M., Birkel, S.D., Saros, J.E., 2019. 2000 years of North Atlantic-Arctic climate. *Quaternary Science Reviews* 216, 1-17.
- Ballabio, C., Panagos, P., Montanarella, L., 2016. Mapping topsoil physical properties at European scale using the LUCAS database. *Geoderma* 261, 110–123.
- Bateman, M.D., 1995. Thermoluminescence dating of British coversand deposits. *Quaternary Science Reviews* 14, 791-798.
- Bateman, M.D., Diez Herrero, A., 2001. The timing and relation of aeolian sand deposition in central Spain to the aeolian sand record of NW Europe. *Quaternary Science Reviews* 20, 779-782.
- Bateman, M.D., Carr, A.S., Dunajko, A.C., Holmes, P.J., Roberts, D.L., McLaren, S.J., Bryant, R.G., Marker, M.E., Murray-Wallace, C.V., 2011. The evolution of coastal barrier systems: A case study of the Middle-Late Pleistocene Wilderness barriers, South Africa. *Quaternary Science Reviews* 30, 63-81.

- 1 Bertran, P., Bateman, M.D., Hernandez, M., Mercier, N., Millet, D., Tastet, J.P., 2011. Inland aeolian
2 deposits of southwest France: facies, stratigraphy and chronology. *Journal of Quaternary Science*
3 26(4), 374-388.
- 4 Bertran, P., Liard, M., Sitzia, L., Tissoux, H., 2016. A map of Pleistocene aeolian deposits in Western
5 Europe, with special emphasis on France. *Journal of Quaternary Science* 31 (8), 844-856.
- 6
7 Björck, S., Clemmensen, L.B., 2004. Aeolian sediment in raised bog deposits, Halland, SW Sweden: a
8 new proxy record of Holocene winter storminess variation in southern Scandinavia? *The Holocene*
9 14(5), 677-688.
- 10
11 Bond, G.C., Lotti, R., 1995. Iceberg discharges into the North Atlantic on millennial time scales during
12 the last glaciation. *Science* 267, 1005-1010.
- 13
14 Bosq, M., Bertran, P., Degeai, J.P., Kreutzer, S., Queffelec, A., Moine, O., Morin, E., 2018. Last Glacial
15 aeolian landforms and deposits in the Rhône Valley (SE France): spatial distribution and grain-size
16 characterization. *Geomorphology* 318, 250-269.
- 17
18 Bosq, M., Bertran, P., Beauval, C., Kreutzer, S., Duval, M., Bartz, M., Mercier, N., Sitzia, L. & the LITAQ
19 project members, 2019. Stratigraphy and chronology of Pleistocene coastal deposits in northern
20 Aquitaine, France: a reinvestigation. *Quaternaire* 30(1), 5-20.
- 21
22 Bosq, M., Kreutzer, S., Bertran, P., sous presse. Chronostratigraphy of two late Pleistocene loess-
23 palaeosol sequences in the Rhône Valley (southeast France). *Quaternary Science Reviews*.
- 24
25 Bourbon, P., 2019. Gestion des eaux souterraines en Région Aquitaine. Carte géologique numérique à
26 1/250 000 de la région Aquitaine. Notice technique. Rapport final, BRGM/RP-68881-FR.
- 27
28 Bressolier, C., Froidefond, J.M., Thomas, Y.F., 1990. Chronology of coastal dunes in the south-west of
29 France. *Catena supplement* 18, 101-107.
- 30
31 Buffault, P., 1942. Histoire des dunes maritimes de la Gascogne. Delmas, Bordeaux, 446 pp.
- 32
33 Cawthra, H.C., Bateman, M.D., Carr, A.S., Compton, J.S., Holmes, P.J., 2014. Understanding Late
34 Quaternary change at the land-ocean interface: A synthesis of the evolution of the Wilderness
35 coastline, South Africa. *Quaternary Science Reviews* 99, 210-223.
- 36
37 Clarke, M.L., Rendell, H.M., Pye, K., 1999. Evidence for the timing of dune development on the
38 Aquitaine Coast, southwest France. *Zeitschrift für Geomorphologie, supplement band* 116, 147-163.
- 39
40 Clarke, M., Rendell, H., Tastet, J.P., Clavé, B., Massé, L., 2002. Late-Holocene sand invasion and North
41 Atlantic storminess along the Aquitaine Coast, southwest France. *The Holocene* 12(2), 231-238.
- 42
43 Costas, S., Jerez, S., Trigo, R.M., Goble, R., Rebêlo, L., 2012. Sand invasion along the Portuguese coast
44 forced by westerly shifts during cold climate events. *Quaternary Science Reviews* 42, 15-28.
- 45
46 De Keyzer, M., Bateman, M.D., 2018. Late Holocene landscape instability in the Breckland (England)
47 drift sands. *Geomorphology* 323, 123-134.
- 48
49 Drăguț, L., Blaschke, T., 2006. Automated classification of landform elements using object-based
50 image analysis. *Geomorphology* 81, 330-344.
- 51
52
53
54
55
56
57
58
59
60
61
62
63
64
65

- 1
2
3
4
5
6
7
8
9
10
11
12
13
14
15
16
17
18
19
20
21
22
23
24
25
26
27
28
29
30
31
32
33
34
35
36
37
38
39
40
41
42
43
44
45
46
47
48
49
50
51
52
53
54
55
56
57
58
59
60
61
62
63
64
65
- Dubreuilh, J., Capdeville, J.P., Farjanel, G., Karnay, G., Platel, J.P., Simon-Coinçon, R., 1995. Dynamique d'un comblement continental néogène et quaternaire: l'exemple du bassin d'Aquitaine. *Géologie de la France* 4, 3–26.
- Frechen, M., Vanneste, K., Verbeeck, K., Paulissen, E., Camelbeeck, T., 2001. The deposition history of coversands along the Bree Fault escarpment, NE Belgium. *Netherlands Journal of Geosciences* 80(3-4), 171-185.
- Froidefond, J.M., Legigan, P., 1985. La grande dune du Pilat et la progression des dunes sur le littoral aquitain. *Bulletin de l'Institut de Géologie du Bassin d'Aquitaine* 38, 69-79.
- Fryberger, S.G., Schenk, C.J., Krystinik, L.F., 1988. Stokes surfaces and the effect of near-surface groundwater-table on aeolian deposition. *Sedimentology* 35, 21-41.
- Goslin, J., Gałka, M., Sander, L., Fruergaard, M., Mokenbusch, J., Thibault, N., Clemmensen, L.B., 2019. Decadal variability of north-eastern Atlantic storminess at the mid- Holocene: New inferences from a record of wind-blown sand, western Denmark. *Global and Planetary Change* 180, 16-32.
- Hanoch, G., Yishak, H., Ashkenazy, Y., 2018. Modeling the bistability of barkhan and parabolic dunes. *Aeolian Research* 35, 9-18.
- Helama, S., Jones, P.D., Briffa, K.R., 2017. Dark Ages Cold Period: A literature review and directions for future research. *The Holocene* 27(10), 1600-1610.
- Iwahashi, J., Pike, R.J., 2007. Automated classifications of topography from DEMs by an unsupervised nested-means algorithm and a three-part geometric signature. *Geomorphology* 86, 409-440.
- Jackson, D.W.T., Costas, S., Guisado-Pintado, E., 2019. Large-scale transgressive coastal dune behavior in Europe during the Little Ice Age. *Global and Planetary Change* 175, 82-91.
- Kasse, C., 1997. Cold-climate aeolian sand-sheet formation in north-western Europe (c. 14-12.4 ka); a response to permafrost degradation and increased aridity. *Permafrost and Periglacial Processes* 8, 295-311.
- Kasse, C., 2002. Sandy aeolian deposits and environments and their relation to climate during the Last Glacial Maximum and Lateglacial in northwest and central Europe. *Progress in Physical Geography* 26, 507–532.
- Kasse, C., Aalbersberg, G., 2019. A complete Late Weichselian and Holocene record of aeolian coversands, drift sands and soils forced by climate change and human impact, Ossendrecht, the Netherlands. *Netherlands Journal of Geosciences* 98, e4 (<https://doi.org/10.1017/njg.2019.3>).
- Kobashi, T., Menviel, L., Jeltsch-Thömmes, A. et coll., 2017. Volcanic influence on centennial to millennial Holocene Greenland temperature change. *Nature Scientific Reports* 7, 1441.
- Kocurek, G., Nielson, J., 1986. Conditions favourable for the formation of warm climate aeolian sand sheets. *Sedimentology* 33, 795-816.
- Koster, E.A., Castel, I.I.Y., Nap, R.L., 1993. Genesis and sedimentary structures of late Holocene aeolian drift sands in northwestern Europe. In K. Pye (ed.), *The dynamics and environmental context of aeolian sedimentary systems*. Geological Society Special Publication 72, 247-267.

1 Kolstrup, E., Murray, A., Possnert, G., 2007. Luminescence and radiocarbon ages from laminated
2 Lateglacial aeolian sediments in western Jutland, Denmark. *Boreas* 36, 314-325.

3 Klingebiel, A., Legigan, P., 1992. Cadre géologique et structure du bassin de la Leyre. *Bulletin de*
4 *l'Institut de Géologie du Bassin d'Aquitaine* 51-52, 7-20.

5
6 Kreutzer, S., Duval, M., Bartz, M., Bertran, P., Eynaud, F., Verdin, F., Mercier, N., 2018. Deciphering
7 coastal dynamics using IR-RF and ESR dating: a case study from Médoc, south-west France.
8 *Quaternary Geochronology* 48, 108-120.

9
10 Legigan, P. 1979. L'élaboration de la formation du Sables des Landes. Dépôt résiduel de
11 l'environnement sédimentaire Pliocène-Pléistocène centre aquitain. *Mémoires de l'Institut de*
12 *Géologie du Bassin d'Aquitaine*, 9.

13
14 Lehmkuhl, F., Zens, J., Krauß, L., Schulte, P., Kels, H., 2016. Loess-paleosol sequences at the northern
15 European loess belt in Germany: Distribution, geomorphology and stratigraphy. *Quaternary Science*
16 *Reviews* 153, 11-30.

17
18 Meszner, S., Kreutzer, S., Fuchs, M., Faust, D., 2013. Late Pleistocene landscape dynamics in Saxony,
19 Germany: Paleoenvironmental reconstruction using loess-paleosol sequences. *Quaternary*
20 *International* 296, 94-107.

21
22 Noppradit, P., Kreutzer, S., Mercier, N., Schmidt, C., Zöller, L., 2015. OSL dating study from the Dune
23 du Pilat in France. Unpublished report, University of Bayreuth.

24
25 Parteli, E.J.R., Durán, O., Herrmann, H.J., 2007. Minimal size of a barkhan dune. *Physical Review E* 75,
26 011301.

27
28 Patton, H., Hubbard, A., Andreasen, K., Auriac, A., Whitehouse, P.L., Stroeven, A.P., Shackleton, C.,
29 Winsborrow, M., Heyman, J., Hall, A.M., 2017. Deglaciation of the Eurasian ice sheet complex.
30 *Quaternary Science Reviews* 169, 148-172.

31
32 Pedersen, K., Clemmensen, L.B., 2005. Unveiling past aeolian landscapes: A ground-penetrating radar
33 survey of a Holocene coastal dunefield system, Thy, Denmark. *Sedimentary Geology* 177, 57-86.

34
35 Pierik, H.J., van Lanen, R.J., Gouw-Bouman, M.T., Groenenwoudt, B.J., Wallinga, J., Hoek, W.Z., 2018.
36 Controls on late-Holocene drift-sand dynamics: The dominant role of human pressure in the
37 Netherlands. *The Holocene* 28(9), 1361-1381.

38
39 Pinto, J.G., Ludwig, P., 2020. Extratropical cyclones over the North Atlantic and western Europe
40 during the Last Glacial Maximum and implications for proxy interpretation. *Climate of the Past* 16,
41 611-626.

42
43 Pontee, N.I., Tastet, J.P., Massé, L., 1998. Morpho-sedimentary evidence of Holocene coastal changes
44 near the mouth of the Gironde and on the Medoc Peninsula, SW France. *Oceanologica Acta* 21(2),
45 243-261.

46
47 Rasmussen, S.O., Bigler, M., Blockley, S.P., Blunier, T., Buchardt, S.L., Clausen, H.B., Cvijanovic, I.,
48 Dahl-Jensen, D., Johnsen, S.J., Fischer, H., 2014. A stratigraphic framework for abrupt climatic
49 changes during the Last Glacial period based on three synchronized Greenland ice-core records:
50 refining and extending the INTIMATE event stratigraphy. *Quaternary Science Reviews* 106, 14-28.

51
52
53
54
55
56
57
58
59
60
61
62
63
64
65

- 1 Sanchez Goñi, M.F., Harrison, S.P., 2010. Millennial-scale climate variability and vegetation changes
2 during the Last Glacial: Concepts and terminology. *Quaternary Science Reviews* 29, 2823–2827.
- 3 Schokke, r J., Koster, E.A., 2004. Sedimentology and facies distribution of Pleistocene cold-climate
4 aeolian and fluvial deposits in the Roer Valley graben (southeastern Netherlands). *Permafrost and*
5 *Periglacial Processes* 15, 1-20.
- 6
7 Schwan, J., 1987. Sedimentologic characteristics of fluvial to aeolian succession in Weichselian
8 Talsand in the Emsland (F.R.G.). *Sedimentary Geology* 52, 273-298.
- 9
10 Serpelloni, E., Faccenna, C., Spada, G., Dong, D., Williams, S.P.D., 2013. Vertical GPS ground motion
11 rates in the Euro-Mediterranean region: New evidence of velocity gradients at different spatial scales
12 along the Nubia-Eurasia plate boundary. *Journal of Geophysical Research: Solid Earth* 118, 6004-
13 6024.
- 14
15
16 Sima, A., Kageyama, M., Rousseau, D.-D., Ramstein, G., Balkanski, Y., Antoine, P., Hatté, C., 2013.
17 Modeling dust emission response to North Atlantic millennial-scale climate variations from the
18 perspective of East European MIS 3 loess deposits. *Climate of the Past* 9, 1385–1402.
- 19
20
21 Sitzia, L., Bertran, P., Bahain, J.J., Bateman, M., Hernandez, M., Garon, H., De Lafontaine, G., Mercier,
22 N., Leroyer, C., Queffelec, A., Voinchet, P., 2015. The quaternary coversands of southwest France.
23 *Quaternary Science Reviews* 124, 84-105.
- 24
25
26 Sitzia, L., Bertran, P., Sima, A., Cherry, P., Queffelec, A., Rousseau, D.D., 2017. Dynamics and sources
27 of last glacial aeolian deposition in southwest France derived from dune patterns, grain-size
28 gradients and geochemistry, and reconstruction of efficient wind directions. *Quaternary Science*
29 *Reviews* 170, 250-268.
- 30
31
32 Smith, B.W., Rhodes, E.J., Stokes, S., Spooner, N.A., Aitken, M.J., 1990. Optical dating of sediments:
33 initial quartz results from Oxford. *Archaeometry* 32(1), 19-31.
- 34
35
36 Spratt, R.M., Lisiecki, L.E., 2016. A Late Pleistocene sea level stack. *Climate of the Past* 12, 1079-1092.
- 37
38 Stéphan, P., Verdin, F., Arnaud-Fassetta, G., Bertrand, F., Eynaud, F., Garcia-Artola, A., Bosq, M.,
39 Culioli, C., Suanez, S., Coutelier, C., Bertran, P., Costa, S., 2019. Holocene coastal changes along the
40 Gironde estuary (SW France): new insights from the North Médoc peninsula beach/dune system.
41 *Quaternaire* 30 (1), 47-75.
- 42
43
44 Strandberg, G., Brandefelt, J., Kjellström, E., Smith, B., 2011. High-resolution regional simulation of
45 last glacial maximum climate in Europe. *Tellus Dynamic Meteorology Oceanography* 63, 107–125.
- 46
47
48 Sun, J, Muhs, D.R., 2013. Dune fields: Mid-Latitudes. In: Elias, S. A. (ed.), *Encyclopedia of Quaternary*
49 *Science*, Second Edition. Elsevier, Amsterdam, pp. 606-622.
- 50
51
52 Tastet, J.P., Pontee, N.L., 1998. Morpho-chronology of coastal dunes in Médoc. A new interpretation
53 of Holocene dunes in Southwestern France. *Geomorphology* 25(1–2), 93-109.
- 54
55
56 Thomas, P.J., Murray, A.S., Granja, H.M., Jain M., 2008. Optical Dating of Late Quaternary Coastal
57 Deposits in Northwestern Portugal. *Journal of Coastal Research* 24(2B), 134-144.
- 58
59
60 Thomas, D.S.G., Bailey, R.M., 2019. Analysis of late Quaternary dunefield development in Asia using
61 the accumulation intensity model. *Aeolian Research* 39, 33-46.
- 62
63
64
65

1 Tolksdorf, J. F., Kaiser, K., 2012. Holocene aeolian dynamics in the European sand-belt as indicated by
2 geochronological data. *Boreas* 41(3), 408-421.

3 Tóth, G., Jones, A., Montanarella, L., European Commission, Joint Research Centre, Institute for
4 Environment and Sustainability, 2013. LUCAS topsoil survey: methodology, data and results. JRC
5 Technical Reports (Publication of the European Union, Luxembourg).

6 Újvári, G., Stevens, T., Molnár, M., Demény, A., Lambert, F., Varga, G., Jull, A.J.T., Páll-Gergely, B.,
7 Buylaert, J.P., Kovács, J., 2017. Coupled European and Greenland last glacial dust activity driven by
8 North Atlantic climate. *Proceedings of the National Academy of Science*,
9 www.pnas.org/cgi/doi/10.1073/pnas.1712651114

10 Van Vliet-Lanoë, B., Penaud, A., Hénaff, A., Delacourt, C., Fernane, A., Goslin, J., Hallégouët, B., Le
11 Cornec, E., 2014. Middle- to late-Holocene storminess in Brittany (NW France): Part II – The
12 chronology of events and climate forcing. *The Holocene* 24(4), 434-453.

13 Van Vliet-Lanoë, B., Lauer, T., Meurisse-Fort, M., Gosselin, G., Frechen, M., 2017. Late Holocene
14 coastal dune activity along the Dover Strait, Northern France – Insights into Middle Ages and Little Ice
15 Age coastal dynamics constrained by optically stimulated luminescence dating. *German Journal of
16 Geology* 68(1), 53-66.

17 Vandenberghe, D.A.G., Derese, C., Kasse, C., Van den haute, P., 2013. Late Weichselian (fluvio-
18)aeolian sediments and Holocene drift-sands of the classic type locality in Twente (E Netherlands): a
19 high-resolution dating study using optically stimulated luminescence. *Quaternary Science Reviews*
20 68, 96-113.

21 Vermeesch, P., 2012. On the visualisation of detrital age distributions. *Chemical Geology* 312, 190–
22 194.

23 Wacha, L., Montanari, A., Lomax, J., Fiebig, M., Lüthgens, C., Korbar, T., Koeberl, C., 2019. Last Glacial
24 Maximum giant sand dunes on the island of Vis, Croatia, in Koeberl C. and Bice D.M. (eds.), 250
25 Million Years of Earth History in Central Italy: Celebrating 25 Years of the Geological Observatory of
26 Coldigioco: Geological Society of America Special Paper 542, pp. 459-470.

27 Walker, M., Head, M.J., Lowe, J., Berkelhammer, L., Björck, S., Cheng, H., Cwynar, L.C., Fisher, D.,
28 Gkinis, V., Long, A., Newnham, R., Rasmussen, S.O., Weiss, H., 2019. Subdividing the Holocene
29 Series/Epoch: formalization of stages/ages and subseries/subepochs, and designation of GSSPs and
30 auxiliary stratotypes. *Journal of Quaternary Science* 34(3), 173-186.

31 Wilson, P., McGourty, J., Bateman, M.D., 2004. Mid- to late-Holocene coastal dune event stratigraphy
32 for the north coast of Northern Ireland. *The Holocene* 14(3), 411-421.

33 Xu, Z., Mason, J.A., Lu, H., 2015. Vegetated dune morphodynamics during recent stabilization of the
34 Mu Us dune field, north-central China. *Geomorphology* 228, 486-503.

35 Zieliński, P., Sokolowski, R.J., Woronko, B., Jankowski, M., Fedorowicz, S., Zaleski, I., Molodkov, A.,
36 Wekwerth, P., 2015. The depositional conditions of the fluvio-aeolian succession during the last
37 climate minimum based on the examples from Poland and NW Ukraine. *Quaternary International*
38 386, 30-41.

Figure captions

Figure 1: Distribution of the coversands, dunes and loess of Aquitaine and location of the sites mentioned in the text. The faults are taken from [Bourbon \(2019\)](#). Profiles P1 and P2 (in red) refer to figure 5. A – Location of the study area, B – Enlargement of the framed area. The Plateau Landais corresponds to the area of low relief covered with sand.

Figure 2: Comparison between the dunes mapped by BRGM (blue line) and according to the method used in this paper (in pink). The DEM is the RGE ALTI® 5 m of IGN. A - Morphology of dunes in the Castets area, B - idem, Biscarosse area, C - idem, Sabres area, D - idem, Rion-des-Landes area. The sites indicated correspond to sites dated by luminescence. BO: blowout, BR: barchanoid ridge, HBR: high barchanoid ridge, IB: isolated barchan, PD: parabolic dune, LPD: low parabolic dune.

Figure 3: Morphology of the coastal dunefield in the Hourtin area. A – Shaded relief and altitude (RGE ALTI® 5 m), B - Satellite view of the framed area (Google Earth, photo 2009). BR: barchanoid ridge, DD: dome dune; IB: isolated barchan, PD: parabolic dune, FSB: foredune sand blanket, PS: Pleistocene surface, MR: megaripples. The dotted line indicates the limit between the coastal dunefield and the Pleistocene surface.

Figure 4: Maximum height (A) and slope (B) of coastal (orange) and inland (blue) dunes. The values were extracted from the RGE ALTI® 5 m.

Figure 5: Stratigraphy of the Miocene to Pleistocene formations of Aquitaine, based on BSS boreholes (<http://infoterre.brgm.fr/>). The location of the profiles is shown in Figure 1 (A: profile P1; B: profile P2). The names of the geological formations are taken from the BSS (cf. [Dubreuilh et al., 1995](#), for the Pleistocene).

Figure 6: Schematic stratigraphy of the new sections observed in trenches and position of dated samples. SW: sand wedge.

Figure 7: Main facies. A – horizontally-bedded sandsheet (ca. 220 ka), with a thin syngenetic sand wedge (Anse-du-Gurp); B – from base to top, horizontally-bedded sandsheet (12.7 ± 0.8 ka) with slightly humic beds, massive sand overlain by a bioturbated humic horizon (Arenosol), then massive dune sand (11.6 ± 0.8 ka, Younger Dryas), St-Geours-de-Maremne; C – massive, bioturbated sand with a buried humic horizon overlying low angle cross-bedded sand (1.86 ± 0.13 ka), parabolic dune at Ondres; D – LIA cross-bedded sands, Dune du Pilat; E – bioturbated massive to horizontally-bedded sand and incipient palaeosols at the base of the dune, Amélie; F – slightly humic convolute beds (0.49 ± 40 ka), Soulac.

Figure 8: Georadar profiles of a parabolic dune at Castets. Borehole BBS002DYHV is taken from the BSS.

Figure 9: Geographical distribution of the age of sand deposits in Aquitaine. A – Middle Pleistocene (> 120 ka), B – Last Glacial (100-30 ka and 30-14 ka), C – Younger Dryas and Holocene.

Figure 10: Chronological distribution of Last Glacial to Holocene OSL ages. KDE: Kernel Density Estimation, CPF - Cumulated Probability Function ([Vermeesch, 2012](#)). The NGRIP ^{18}O curve is taken from [Rasmussen et al \(2014\)](#). The Heinrich Events (Hes) are from [Sanchez Goñi and Harrison \(2010\)](#).

Figure 11: A - Chronological distribution of OSL ages between 14 ka and 0 ka; KDE: Kernel Density Estimation, CPF - Cumulated Probability Function ([Vermeesch, 2012](#)); B - idem, IRSL ages, from [Clarke et al. \(1999, 2002\)](#). The DACP and LIA are from [Helama et al. \(2017\)](#) and [Kobashi et al. \(2017\)](#).

Figure 12: Maximum slope of the dunes dated by OSL. The slope values were taken from the RGE ALTI® 5 m.

Table 1: New OSL ages obtained in this study.

Table 2: List of the ages of aeolian sands used in this study.

Supplementary Information: Dating methodology (including recalculated ages).

1
2
3
4
5
6
7
8
9
10
11
12
13
14
15
16
17
18
19
20
21
22
23
24
25
26
27
28
29
30
31
32
33
34
35
36
37
38
39
40
41
42
43
44
45
46
47
48
49
50
51
52
53
54
55
56
57
58
59
60
61
62
63
64
65

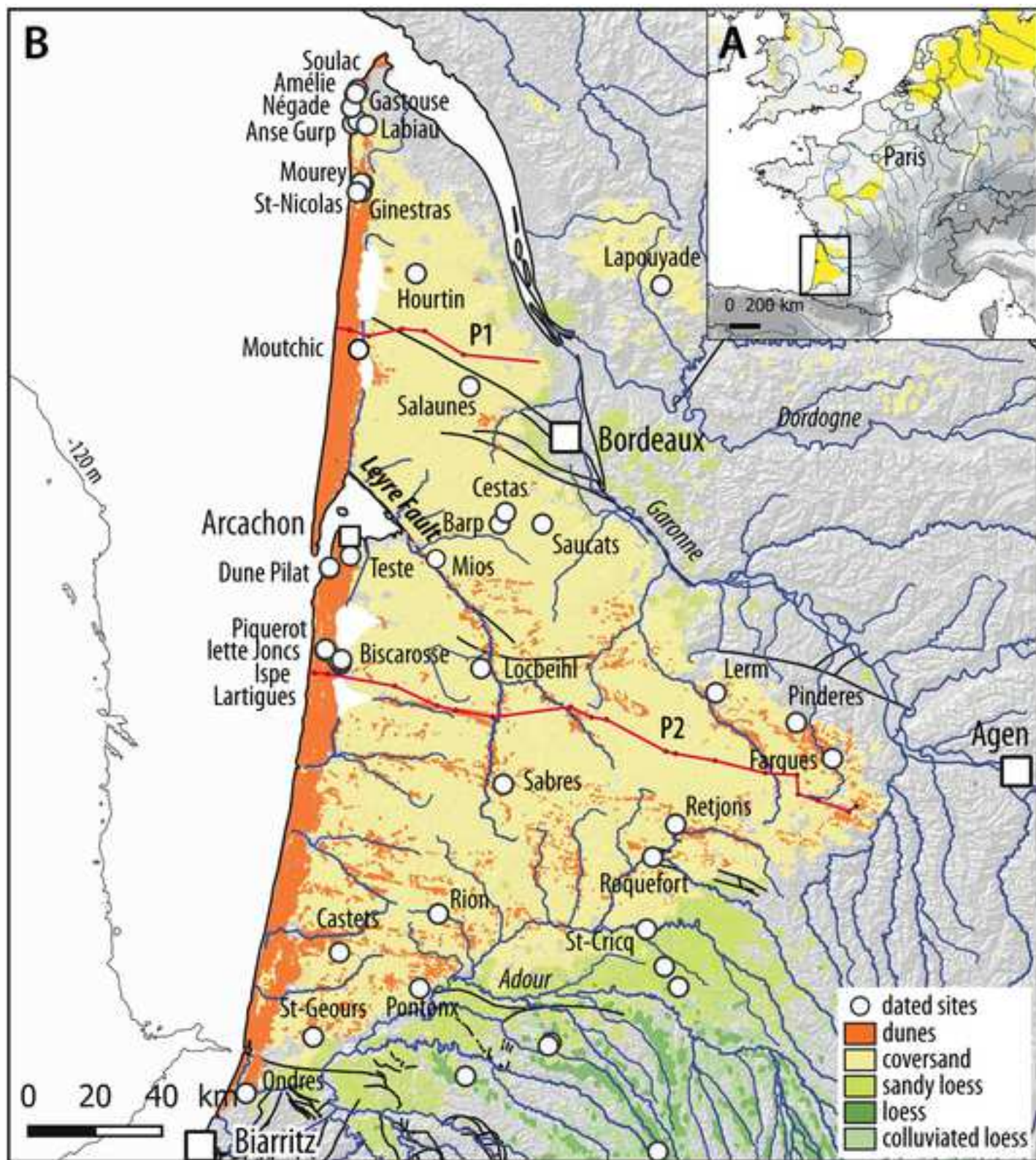
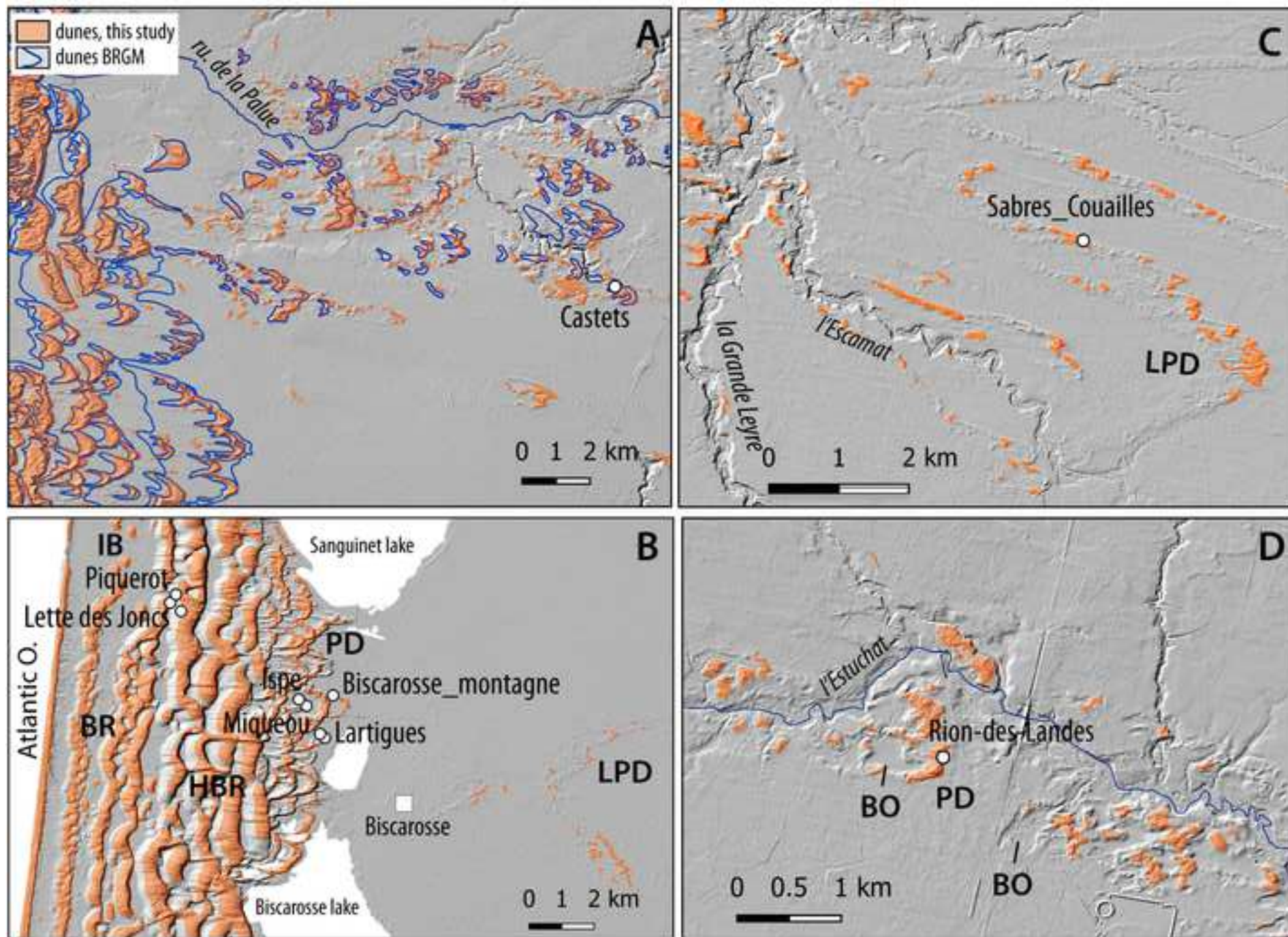
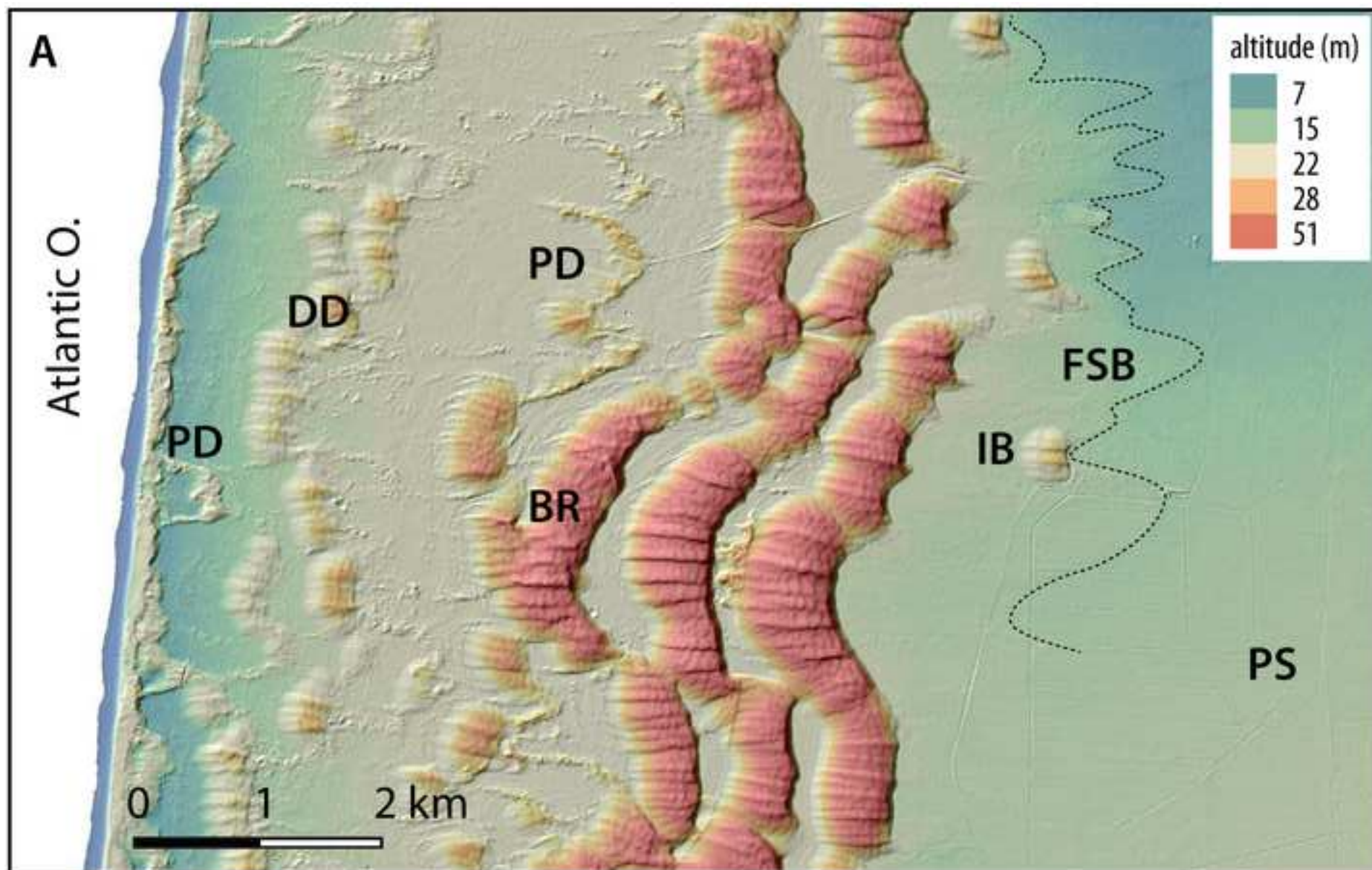
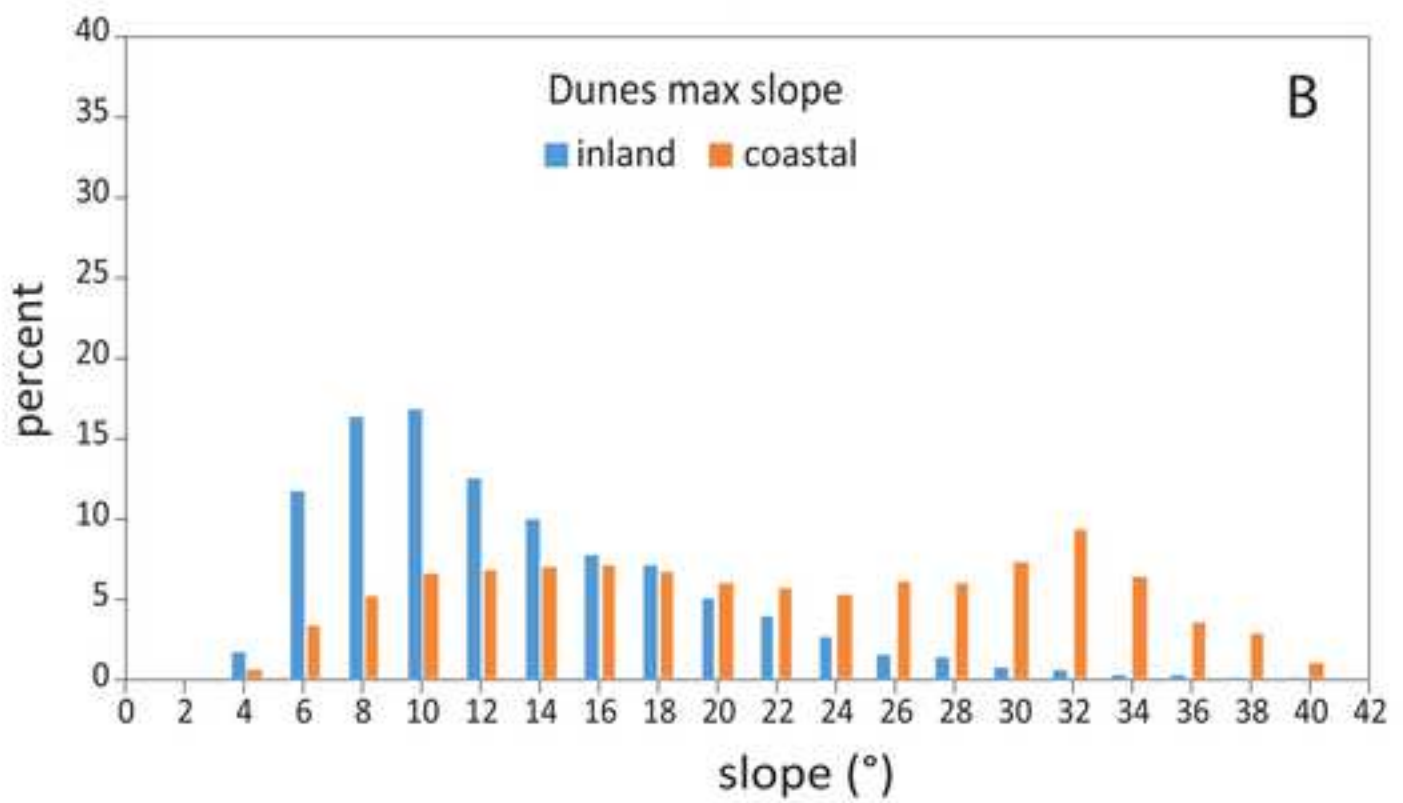
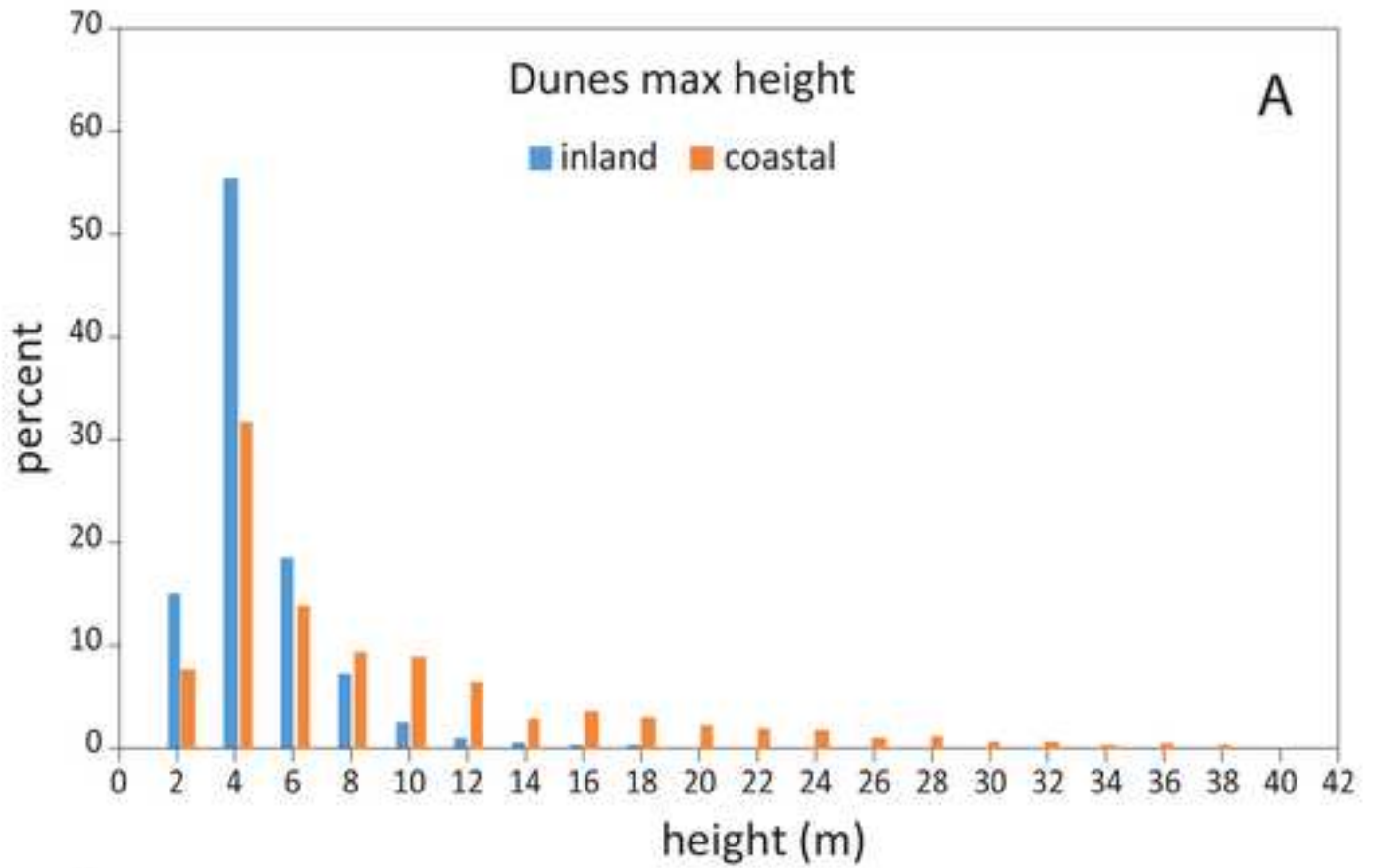


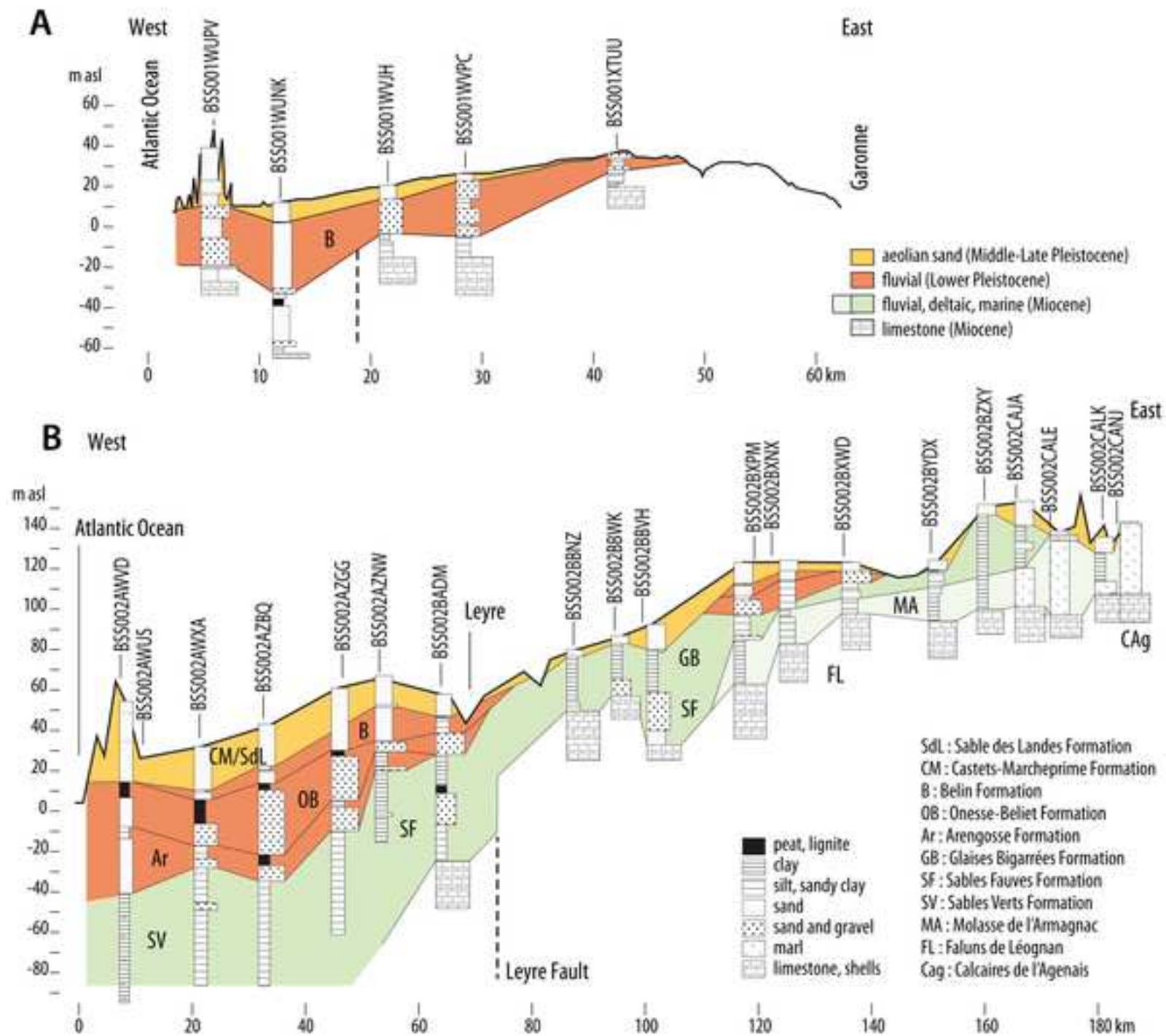
Figure 2

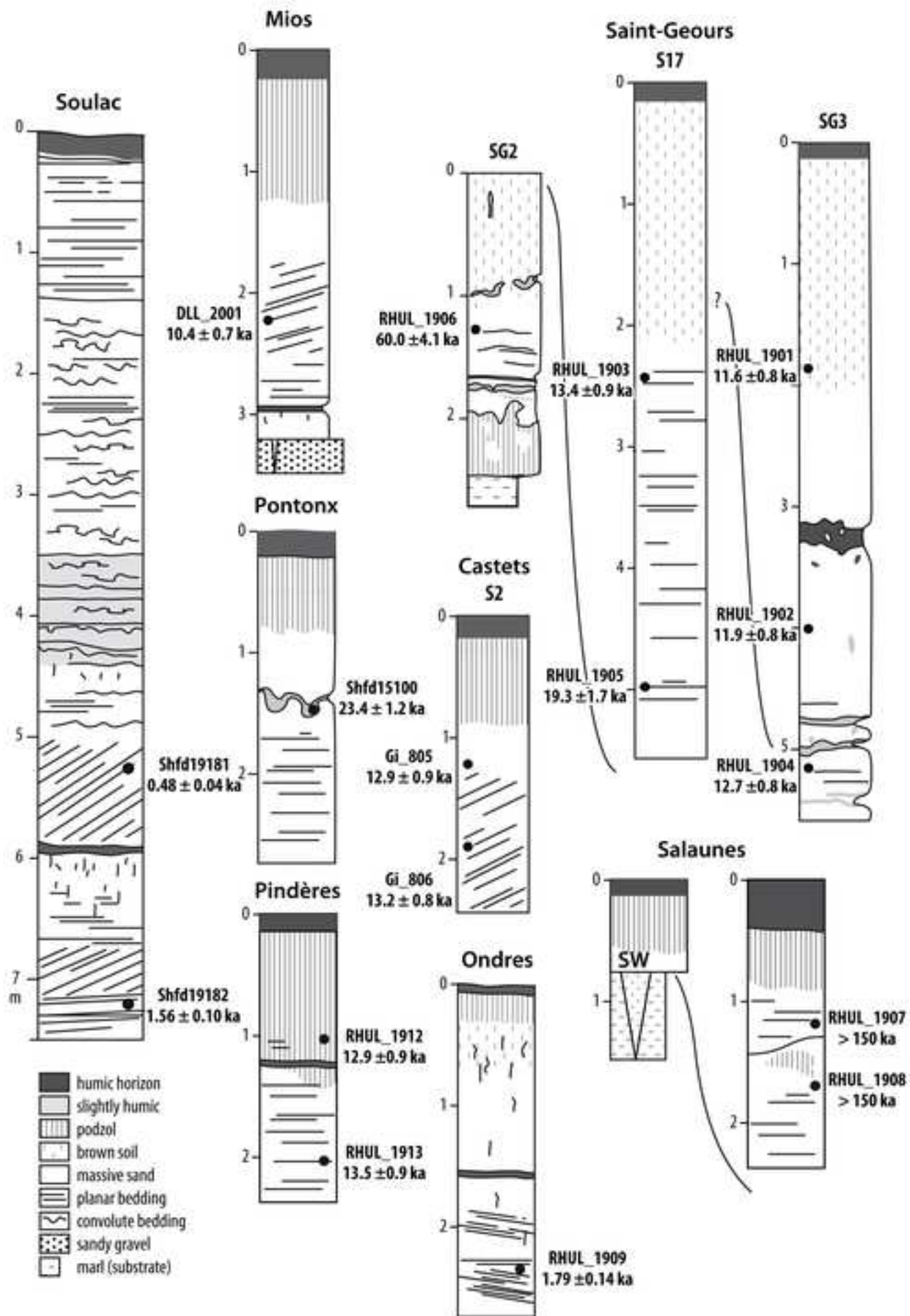
[Click here to access/download;Figure;Fig02 Dunes Biscarosse_Sabres_Rion2.jpg](#)

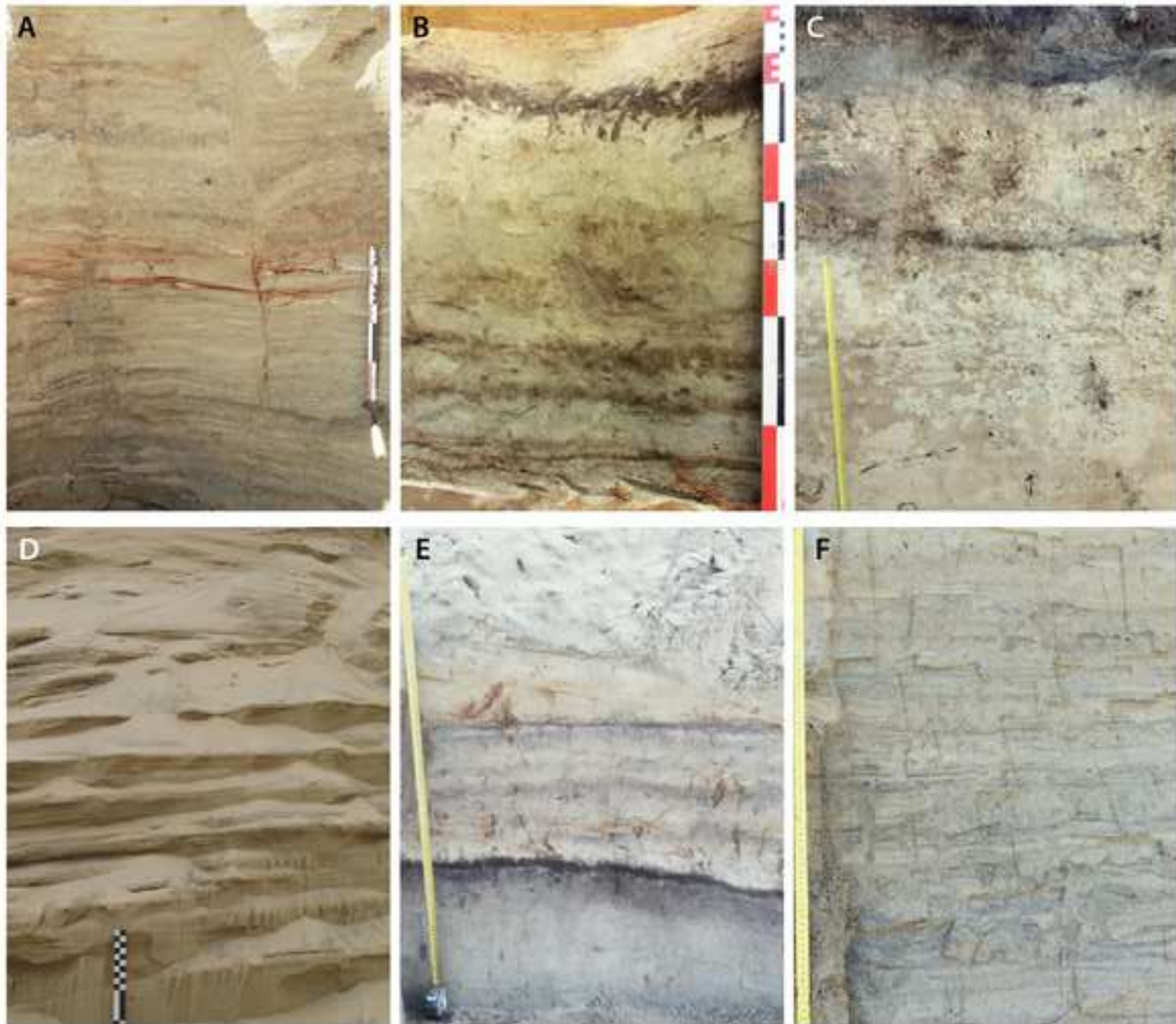


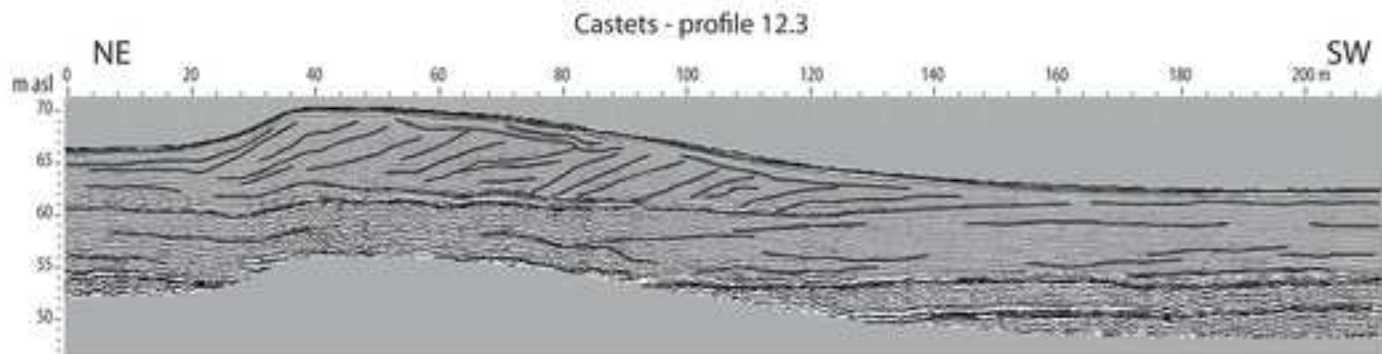
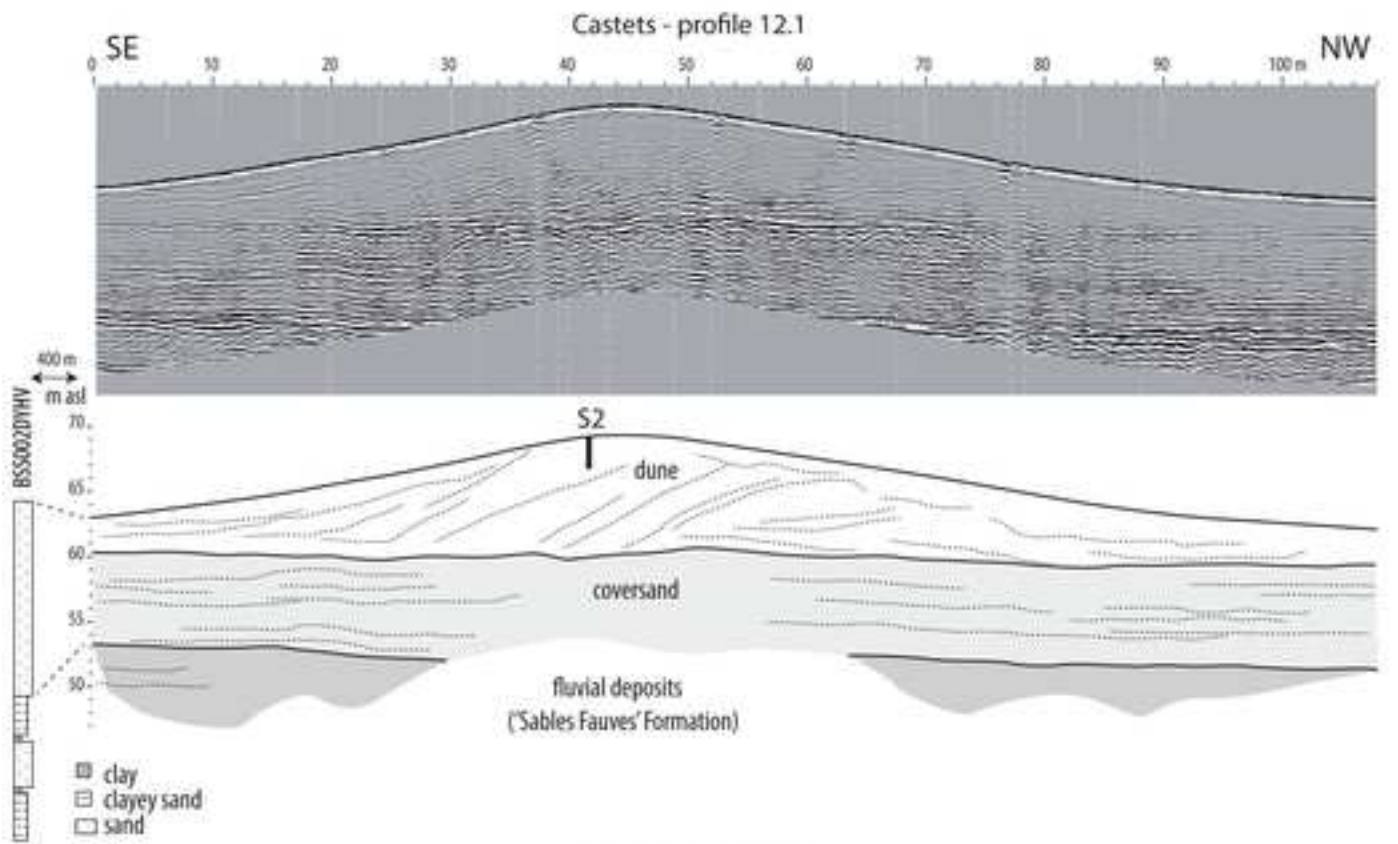
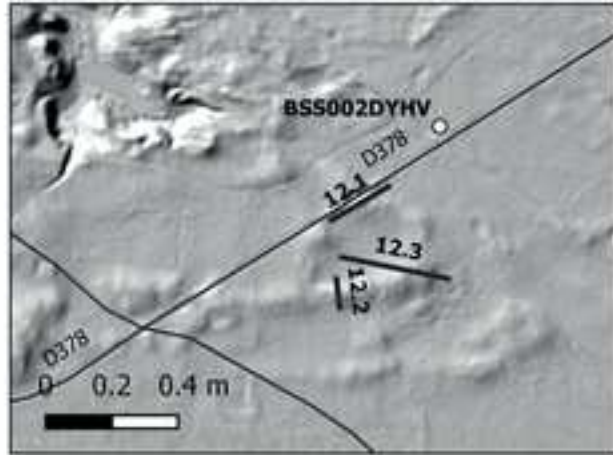












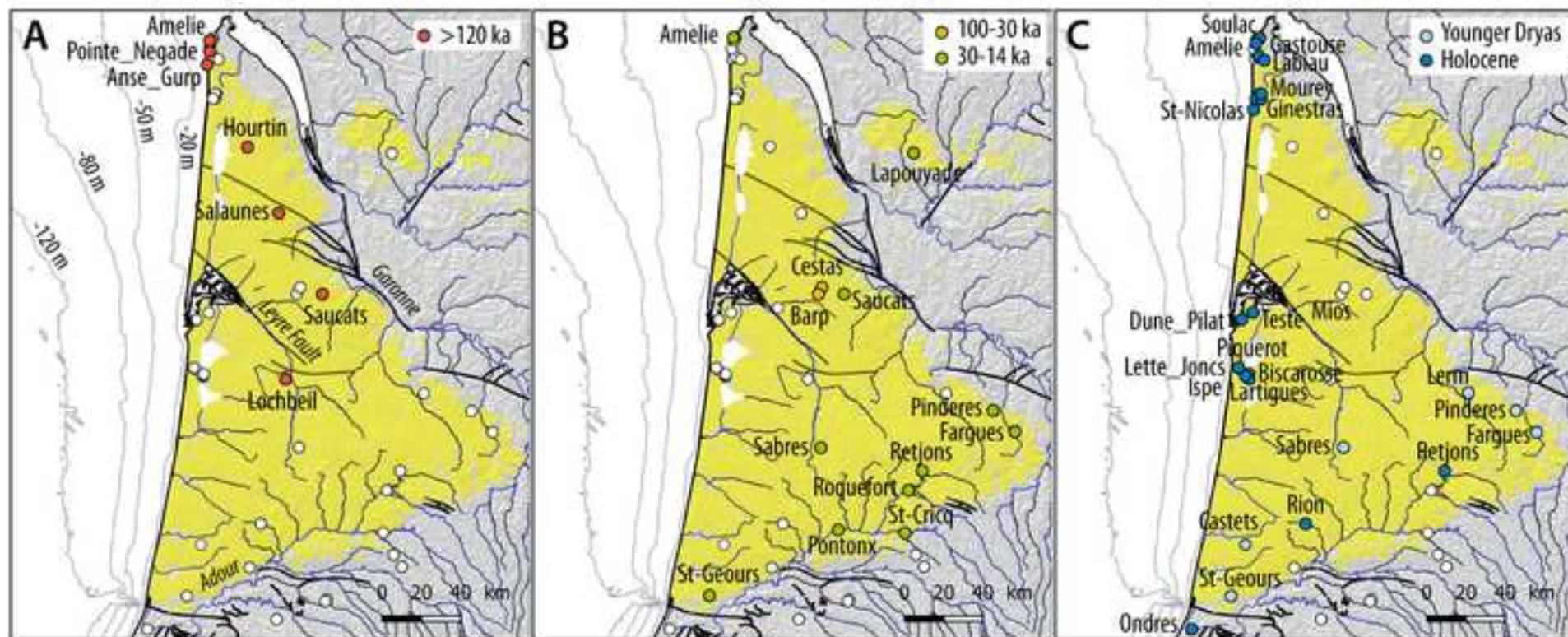


Figure 10

